Threshold effects in photodetachment near an autodetaching or excited-state resonance

S. L. Haan and M. Walhout*
Department of Physics, Calvin College, Grand Rapids, Michigan 49546

J. Cooper
Joint Institute for Laboratory Astrophysics,
University of Colorado and National Institute for Standards and Technology, Boulder, Colorado 80309-0440
(Received 14 July 1989)

Near-threshold photodetachment processes are considered for a simple model system that represents a negative ion that supports an excited state close to the threshold of a single-electron continuum. The excited state is assumed to be autodetaching if it lies above the threshold. Expressions for the discrete-state–discrete-state matrix elements of the Green's operator are derived and are used to obtain a solution of the time-dependent Schrödinger equation which is exact within the model. The weak-field resonance profile is presented, and the importance of terms that are neglected in the usual pole approximation is discussed. The time development of the populations and shifts of threshold are discussed for stronger fields. Population trapping through threshold shifts and through interference effects are considered. The possibility of meeting both trapping conditions simultaneously is discussed.

I. INTRODUCTION

There have been a number of theoretical investigations of threshold effects in the photoionization of neutral atoms[1–3] and the photodetachment of negative ions.[4–13] The two situations are, of course, different in that neutral atoms support a Rydberg series of bound states below the threshold of the continuum, while negative ions have a density of continuum states going to zero at threshold, and no Rydberg series. It is the latter case that is of interest in the present work.

Among the effects predicted for negative ions exposed to strong laser fields are a dynamic photodetachment threshold and nonexponential "decay" of the discrete state by photoabsorption. For example, Cohen-Tannoudji and Avan[4] have discussed in a general context the shift of the decaying state that can arise because of the interaction with the continuum, and the partial stabilization of the system which can occur if the discrete state is shifted below the threshold of the continuum. They have also discussed how, with increasing coupling strength, the exponential decay of the discrete state is changed into damped oscillations between the discrete state and the continuum.

It has been predicted[10] that the size of the Stark shift of the initially populated discrete state relative to the threshold of the continuum will be directly proportional to the laser intensity, with constant of proportionality typically being of order 10^{-10} $\mathrm{cm}^{-1}/(\mathrm{W/cm}^2)$. It has also been suggested that the effects could be enhanced in negative ions featuring an autodetaching state near the threshold of the continuum. For example, Voitkiv and Pazdzersky[12] have considered threshold photodecay of negative ions into s-wave and into p-wave continua in the presence of a low-lying autodetaching state, and have shown that the autodetaching state strongly affects the photodetachment process.

It is also generally accepted that a full description of threshold effects in photoionization or photodetachment must account not only for the ac Stark shift, but also for the "quiver energy" or "ponderomotive shift" of the detached electron in the oscillating, externally applied field.[13,14] A dynamic threshold for photodetachment has been observed experimentally by Trainham *et al.*,[15] who used a low-frequency, high-intensity laser to generate the shift, and used a high-frequency, low-intensity laser for the photodetachment.

There have also been a number of studies of strong-field effects in atomic systems supporting autoionizing states that are far from threshold.[16–30] One of the predictions of these studies of laser-induced autoionization is a line-narrowing effect. This effect can be thought of as arising through quantum-mechanical interference effects similar to those that give rise to the Fano minimum[31] in weak-field photoionization near autoionizing resonances. In model studies which do not take into account any of the various background processes which can give rise to photoionization, this line-narrowing effect becomes a population trapping effect in which some of the population of the discrete states never decays into the continuum.

Thus population trapping effects have been considered in model systems within two quite different contexts, namely through threshold shifts and through interference effects in laser-induced autoionization. Other studies have discussed the possibility of trapping arising in systems in which continuum structure can be provided by a high-intensity laser instead of[32–34] or in addition to[34–38] the autoionizing state which provides the continuum structure in laser-induced autoionization.

In the present work we study photodetachment within a simple model system representing a negative ion in an

external, monochromatic laser field. The negative ion is assumed in this work to support an autodetaching or excited state close to the threshold of the continuum. We choose a particular energy dependence for the discrete-state–continuum matrix elements of the Hamiltonian, and we find exact expressions for the matrix elements of the discrete-state space Green's operator and of the time-dependent Schrödinger equation for the model. These expressions are used to show explicitly the well-known conclusion that the "pole approximation" is not valid in the vicinity of the threshold of a continuum in systems featuring no Rydberg states. The expressions are also used to study the time development of the system and to consider population trapping occurring through either or both of threshold shifts and quantum-mechanical interference effects.

In this work we present an analysis of a model system only, and no effort is made to model any particular real negative atoms. However, rather than working with arbitrary energy and intensity units throughout this work, we will work in conventional units, such as electron volts and wave numbers for energies. Parameter sizes will be chosen so as to illustrate clearly the effects of interest in this work, and without reference to any particular atoms. The energies and intensities presented can, of course, easily be scaled to other values as long as various ratios are kept constant.

In Sec. II of this paper we describe our model in detail, and we derive exact expressions for discrete-state–discrete-state matrix elements of the Green's operator for our model system. We also discuss some of the processes that have been ignored in choosing the model. In Sec. III we discuss the limitations of the pole approximation in the context of the Fano q parameter and the Fano line profile. In Sec. IV we present the solution of the time-dependent Schrödinger equation, and use it to study strong-field effects in the time development of the detachment probability and population trapping. Included is a discussion of how certain of the poles of the initial-state–initial-state matrix element of the Green's operator can be interpreted as representing decaying dressed states. The stabilization of these states via shifting below the threshold of the continuum and via interference effects is discussed in detail. Finally, in Sec. V we present a summary and a discussion of our results.

II. PRESENTATION OF MODEL AND FORMALISM

We assume that the Hamiltonian for the system has been decomposed as $H=H^A+H^F+V$, where H^A denotes the atomic Hamiltonian in the absence of configuration interaction, H^F denotes the Hamiltonian of the radiation field, and V represents the sum of the atom-field interaction and configuration interaction. The eigenstates of H^A and the couplings between them are shown in Fig. 1. The "unperturbed energy eigenstates" of the model negative ion consist of two discrete states and one electron continuum. One discrete state, denoted by $|1\rangle_A$, represents a bound state of the negative ion, and is assumed to be the initial state. The second discrete state $|2\rangle_A$ has energy close to the energy threshold of the continuum. The continuum $\{|E\rangle_A\}$ corresponds to an unbound electron and neutral atomic core. For definiteness, the electron continuum is assumed to be an s-wave continuum. The bound discrete state $|1\rangle_A$ is coupled to the other discrete state and to the continuum by a monochromatic laser. The second discrete state is assumed to be coupled to the continuum by configuration interaction. When its energy is above the continuum threshold, the state is autodetaching. (One then could think in terms of the upper state and the continuum together forming a structured continuum, but throughout this work we will think of the upper state as separate from the continuum.) The eigenstates of H^A+H^F are taken to be product states of the atomic kets and photon-number kets

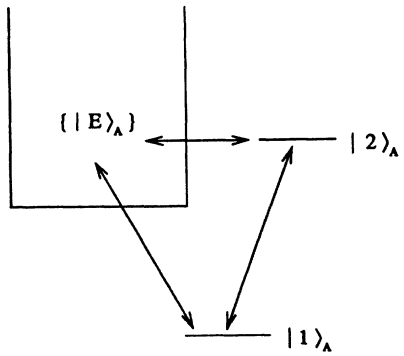

FIG. 1. Schematic diagram of the energy eigenstates of H^A and of the couplings that arise through the interactions considered.

$$
\begin{aligned}
|1\rangle &\equiv |1\rangle_A |N\omega\rangle \ , \\
|2\rangle &\equiv |2\rangle_A |(N-1)\omega\rangle \ , \\
|E\rangle &\equiv |E\rangle_A |(N-1)\omega\rangle \ ,
\end{aligned}
\tag{2.1}
$$

where ω denotes the laser frequency. We write the energies of states $|1\rangle$, $|2\rangle$, and $|E\rangle$ by E_1, E_2, and E, respectively, and we define the zero of energy to be the threshold (lowest energy) of the continuum $\{|E\rangle\}$. Because of this choice of zero, changing the laser frequency changes E_1, but not E_2 or the continuum energies $\{E\}$; E_1 thus serves as a laser frequency parameter, giving the energy of the initial state plus one laser photon, relative to the threshold of the continuum. We also assume that $\langle i|j\rangle=\delta_{ij}$, $\langle j|E\rangle=0$ $(i,j=1,2)$, and that the continuum states have been normalized to a δ function in energy: $\langle E|E'\rangle=\delta(E-E')$.

We assume the following form for the matrix elements of V coupling the discrete states to the continuum:

$$
|V_{jE}|^2=\frac{2}{\pi}\beta_j^{3/2}A_j\frac{E^{1/2}}{(E+\beta_j)^2}, \quad j=1,2 \ . \tag{2.2}
$$

The β parameters are continuum-width parameters, and have dimensions of energy. The parameters A_1 and A_2 are coupling strength parameters, and also have dimensions of energy. (Thus all dependence of V_{1E} on laser

photon number N, and correspondingly on laser intensity, is absorbed into A_1.) Close to threshold, the couplings (2.2) exhibit the $E^{1/2}$ energy dependence of the Wigner theory[39] for couplings to an s-wave continuum. We furthermore assume that each V_{jE} is real and positive. This assumption can be made in the model without loss of essential generality, provided we allow the discrete-state–discrete-state coupling to be either positive or negative.

The time-dependent Schrödinger equation for the above system can be solved without further approximation. The populations of the discrete states at time t are $|\langle 1|\psi(t)\rangle|^2$ and $|\langle 2|\psi(t)\rangle|^2$ [with $|\psi(0)\rangle=|1\rangle$], where

$$\langle j|\psi(t)\rangle=\frac{1}{2\pi i}\int_c dz\, e^{-izt}\langle j|G(z)|1\rangle, \quad j=1,2\ . \tag{2.3}$$

Here $G(z)$ denotes the Green's operator, or resolvent, defined in the complex plane by $G(z)=(z-H)^{-1}$. The contour of integration c in (2.3) is in the upper half plane, from $+\infty+i0$ and $-\infty+i0$.

In order to write expressions for the matrix elements of the Green's operator appearing in (2.3), we first define projection operators

$$\begin{aligned} P&=\int dE|E\rangle\langle E|\ , \\ Q&=|1\rangle\langle 1|+|2\rangle\langle 2|\ . \end{aligned} \tag{2.4}$$

One then can show[40] that

$$\begin{aligned} QG(z)Q&=Q\{Q[z-H^0-\Lambda(z)]Q\}^{-1}\ , \\ \Lambda(z)&=V+VP[P(z-H^0-V)P]^{-1}V\ . \end{aligned} \tag{2.5}$$

For our model $PVP=0$ (i.e., we neglect the continuum-continuum coupling) and $QG(z)Q$ is the inverse of the simple 2×2 matrix

$$Q[z-H^0-\Lambda(z)]Q=\begin{bmatrix} z-E_1-\Sigma^{11}(z) & -V_{12}-\Sigma^{12}(z) \\ -V_{21}-\Sigma^{21}(z) & z-E_2-\Sigma^{22}(z) \end{bmatrix}, \tag{2.6}$$

where the Σ^{ij} represent the various self-energies

$$\begin{aligned} \Sigma^{ij}(z)&=\langle i|VP(z-H^0)^{-1}PV|j\rangle \\ &=\int_0^\infty dE\frac{\langle i|V|E\rangle\langle E|V|j\rangle}{z-E}\ . \end{aligned} \tag{2.7}$$

Thus

$$\begin{aligned} QG(z)Q=\{&[z-E_1-\Sigma^{11}(z)][z-E_2-\Sigma^{22}(z)] \\ &-[V_{12}+\Sigma^{12}(z)][V_{21}+\Sigma^{21}(z)]\}^{-1} \\ &\times\begin{bmatrix} z-E_2-\Sigma^{22}(z) & V_{12}+\Sigma^{12}(z) \\ V_{21}+\Sigma^{21}(z) & z-E_1-\Sigma^{11}(z) \end{bmatrix}. \end{aligned} \tag{2.8}$$

For our model couplings, we use Ref. 41 and techniques discussed in Ref. 10 to obtain

$$\Sigma^{jj}(z)=\frac{-\beta_j A_j}{[-iz^{1/2}+(\beta_j)^{1/2}]^2}\ , \tag{2.9a}$$

$$\Sigma^{12}(z)=\Sigma^{21}(z)=\frac{-2(\beta_1\beta_2)^{3/4}(A_1A_2)^{1/2}}{[-iz^{1/2}+(\beta_i)^{1/2}][-iz^{1/2}+(\beta_j)^{1/2}][(\beta_i)^{1/2}+(\beta_j)^{1/2}]}\ . \tag{2.9b}$$

(We have written these in terms of $-iz^{1/2}$ in anticipation of defining the variable $y=-iz^{1/2}$ in Sec. IV.) We note from (2.9) that $\Sigma^{jj}(0)=-A_j$.

Before presenting any numerical results, we comment briefly upon the approximations that have been made in choosing the model. We have neglected processes such as continuum-continuum transitions, photoabsorption from the autodetaching state, photoabsorption from the initial state into an alternative continuum, and spontaneous radiative decay. We have also made the rotating-wave approximation throughout the work.

Because we neglect all continuum-continuum couplings, we cannot expect the present work to describe properly the strong-field effects that can arise for continuum electrons or above threshold ionization effects. More specifically, the present model does not account for any quiver energy[13,14] or ponderomotive shift of the continuum electron. This is not a serious drawback of the model, however, provided we keep our laser intensities small enough that the ponderomotive energy is small. The ponderomotive shift is directly proportional to the laser intensity, and for photon energies of order 1 eV (such as will be of interest in this work) the ponderomotive shift is approximately 10^{-9} cm^{-1}/(W/cm^2). In the present work we shall limit ourselves to intensities of order 10^{10} W/cm^2 or less so that the ponderomotive shift is of order 10 cm^{-1} or less. The lowest energy of the continuum will remain at all times at our zero of energy, and "threshold shifts" will occur in the present work only in the sense that one discrete state is shifted below the lowest energy of the continuum.

Two processes which prevent population trapping from occurring, and which give a minimum width to the decaying dressed states, are photoabsorption from the autodetaching state and spontaneous radiative decay. The former process has been discussed within the context of laser-induced autoionization by Andryushin *et al.*[20] It also was included in the studies done by Voitkiv and Pazdzersky.[12] The latter process has been studied by a number of authors,[25–30] and can give rise to interesting recycling effects. Of course, a major difference between these two processes is that photoabsorption scales with the laser intensity. The projected Green's operator $QG(z)Q$ can be adjusted to take these processes into account. For z in the vicinity of E_1 and E_2, the photoabsorption can be included in $QG(z)Q$ through the simple

substitution of $E_2 - iI\xi/2$ for E_2, where I is the laser intensity and $I\xi$ is 2π times the modulus squared of the matrix element of the Hamiltonian between $|2\rangle$ and the photoabsorption continuum. Similarly, one-photon spontaneous radiative decay from $|2\rangle$ can be accounted for through the addition of $-i\gamma/2$ to E_2, where γ is the radiative decay rate of $|2\rangle$. Spontaneous radiative decay from the electron continuum can also be taken into account, for z in the vicinity of E_1 and E_2, by minor revision of $QG(z)Q$.[38,40,42] These processes would need to be accounted for in modeling real atoms.

A first-order correction to the rotating-wave approximation can be obtained by substituting $E_1 - \Sigma^{11}(-2\omega)$ for E_1 in the formalism.[9,10] The size of this shift is proportional to and less than A_1, and in our model depends on the value of β_1. More generally, the precise character of the shift introduced by the counterrotating term depends on the structure of the entire continuum, which our simple model couplings do not take into account. Because of the smallness of the shift, as well as the inability of our model couplings, which were chosen to model threshold behavior, to account for details in the structure of the entire continuum, we have not included any correction to the rotating-wave approximation in our analysis.

III. POLE APPROXIMATION DISCUSSION

In many works involving the decay of prepared systems, one makes the pole approximation (PA), which, in the present context, is equivalent to neglecting the real parts of the various self-energies. (One form of the PA is to treat the real parts of the self-energies as constants in energy, but throughout this work we will take the PA to consist of the more extreme approximation of neglecting the real parts entirely.) Because we have exact expressions for the self-energies within this model system, we are able to examine closely the validity of the pole approximation within various contexts. For example, the Fano q parameter is given by[31,42]

$$q(E)=\frac{\mathrm{Re}\Lambda_{12}(E+i0)}{-\mathrm{Im}\Lambda_{12}(E+i0)}=\frac{V_{12}+\mathrm{Re}\Sigma^{12}(E+i0)}{\pi V_{1E}V_{E2}} . \quad (3.1)$$

For our couplings we have from (2.9)

$$\mathrm{Re}\Sigma^{12}(E\pm i0)=\frac{-2(\beta_1^{3/2}\beta_2^{3/2})^{1/2}A_1A_2[(\beta_1\beta_2)^{1/2}-E]}{[(\beta_1)^{1/2}+(\beta_2)^{1/2}]\{[(\beta_1\beta_2)^{1/2}-E]^2+E[(\beta_1)^{1/2}+(\beta_2)^{1/2}]^2\}} . \quad (3.2)$$

In the PA, one neglects the term $\mathrm{Re}\Sigma^{12}(E+i0)$ relative to V_{12} in the expression for q, and writes simply

$$q(E)_{\mathrm{PA}}=\frac{V_{12}}{\pi V_{1E}V_{E2}} . \quad (3.3)$$

The pole approximation is well known not to be valid near a continuum threshold. This conclusion is illustrated in Fig. 2, where we compare the full q parameter as given by (3.1) with the pole approximation q given by (3.3) for a case in which $0<V_{12}<|\mathrm{Re}\Sigma^{12}(0+i0)|$. We note that

$$\mathrm{Re}\Sigma^{12}(0+i0)=\frac{-2A_1A_2}{(\beta_1\beta_2)^{1/4}[(\beta_1)^{1/2}+(\beta_2)^{1/2}]} , \quad (3.4)$$

is always negative, so that for this case, q and q_{PA} have different signs close to threshold. The plots are equal at only one point, that being at $E=(\beta_1\beta_2)^{1/2}$. The plots clearly show the possible importance of $\mathrm{Re}\Sigma^{12}$ in evaluating q at energies close to threshold.

The limitations of the pole approximation can also be

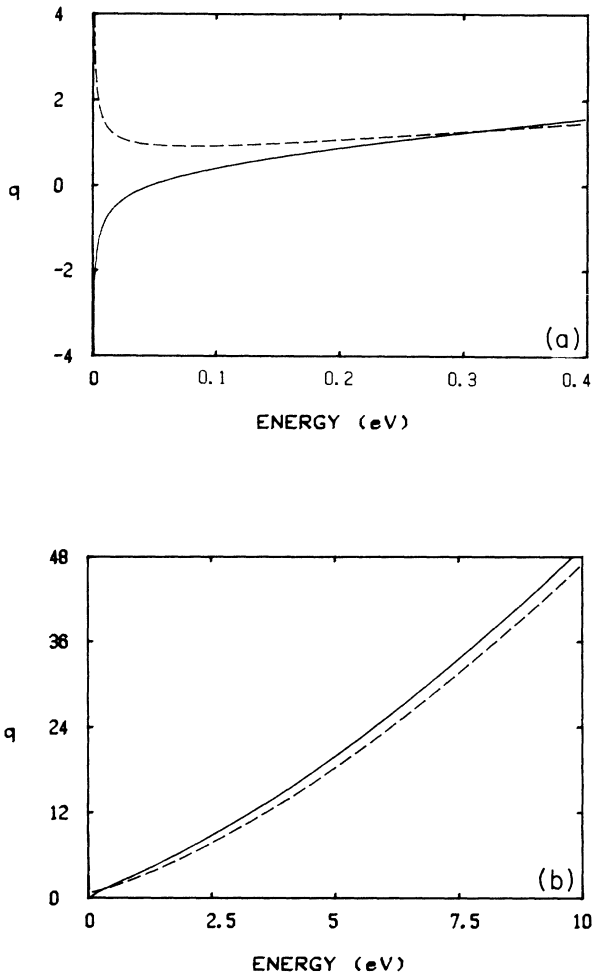

FIG. 2. Fano q parameter vs continuum energy as given by Eqs. (3.1) (solid) and (3.3) (dashed). The pole approximation has not been made in the former case, but has in the latter. (a) is a closeup of the low-energy region of (b). Various parameters have been set as follows: $A_2=100$ cm^{-1}, $\beta_1=1$ eV, $\beta_2=0.1$ eV, $A_1/I=2\times10^{-10}$ cm^{-1}/(W/cm^2), $V_{12}/\sqrt{I}=6.73\times10^{-5}$ cm^{-1}/(W/cm^2)$^{1/2}$.

examined in the context of the resonance profile of the autodetaching state, which is given by[31]

$$S_F(\varepsilon)=\frac{[\varepsilon(E)+q(E)]^2}{1+\varepsilon(E)^2}\ , \tag{3.5a}$$

$$\varepsilon=\frac{E-E_2-\mathrm{Re}\Lambda_{22}(E+i0)}{-\mathrm{Im}\Lambda_{22}(E+i0)}\ . \tag{3.5b}$$

In the pole approximation one neglects the $\mathrm{Re}\Lambda_{22}(E+i0)$ appearing in the definition of ε, and uses q_{PA} rather than q. Figure 3 shows the resonance profile as given by (3.5a) both with and without the pole approximation. The parameters are the same as for Fig. 2. Both the curvature of the profile and the energy of the Fano minimum are modified by the PA. It should be noted that the appropriateness of the PA may be improved with different atomic parameters. However, a solution to the general problem of an autoionizing state near threshold should ideally be obtained without making the PA.

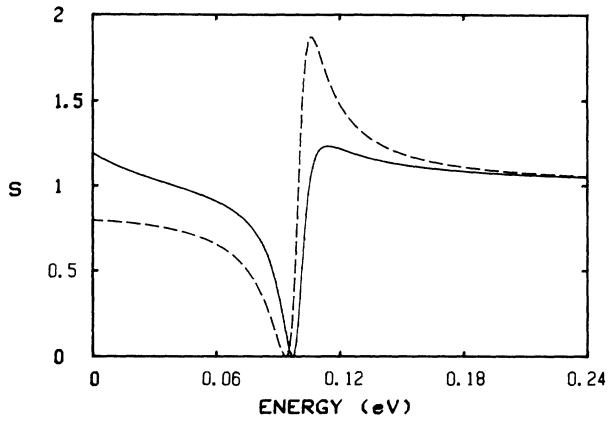

FIG. 3. Fano profiles with (dashed) and without (solid) the pole approximation for an autoionizing state near threshold differ in shape and in their predictions of the energy of the Fano minimum. The autodetaching state has energy $E_2=0.1$ eV. Other parameters are the same as in Fig. 2.

IV. TIME DEVELOPMENT AND STRONG-FIELD EFFECTS

Using the methods described elsewhere[10] the time t population amplitude for the two discrete states can be written, after the change of variable $y=-iz^{1/2}$ to eliminate fractional powers and multiple Riemann sheets,

$$\langle 1|\psi(t)\rangle=\frac{1}{\pi i}\sum_j\frac{N(y_j)}{D'(y_j)}\int_{c'}dy\frac{e^{iy^2t}}{y-y_j} \tag{4.1a}$$

$$=\sum_j\frac{N(y_j)}{D'(y_j)}W(y_j\sqrt{t}\,e^{-i\pi/4})\ , \tag{4.1b}$$

$$\langle 2|\psi(t)\rangle=\frac{1}{\pi i}\sum_j\frac{S(y_j)}{D'(y_j)}\int_{c'}dy\frac{e^{iy^2t}}{y-y_j} \tag{4.1c}$$

$$=\sum_j\frac{S(y_j)}{D'(y_j)}W(y_j\sqrt{t}\,e^{-i\pi/4})\ . \tag{4.1d}$$

In (4.1a) and (4.1c) the contour of integration c' in the y plane runs from $-i\infty$ on the negative imaginary axis, to the origin, then along the positive real axis to $+\infty$. Any poles encountered along these axes are to be avoided by moving into the fourth quadrant. The quantities $N(y)$, $S(y)$, and $D(y)$ are given below. The y_j in Eq. (4.1) represent zeros of $D(y)$, and $D'(y)$ represents the derivative of $D(y)$. The W function is closely related to the complementary error function.[43] The functions N, S, and D are, letting $r=2(\beta_1\beta_2)^{1/4}/[(\beta_1)^{1/2}+(\beta_2)^{1/2}]$,

$$N(y)=-y[y+(\beta_1)^{1/2}]^2\{A_2\beta_2-[y+(\beta_2)^{1/2}]^2(y^2+E_2)\}\ , \tag{4.2}$$

$$S(y)=-y\{V_{12}[y+(\beta_1)^{1/2}]^2[y+(\beta_2)^{1/2}]^2-r[y+(\beta_1)^{1/2}][y+(\beta_2)^{1/2}](A_1A_2\beta_1\beta_2)^{1/2}\}\ , \tag{4.3}$$

$$\begin{aligned}D(y)=&y^8\{1\}+y^7\{2[(\beta_1)^{1/2}+(\beta_2)^{1/2}]\}+y^6\{E_1+E_2+\beta_1+\beta_2+4(\beta_1\beta_2)^{1/2}\}\\
&+y^5\{2\{(\beta_1)^{1/2}\beta_2+(\beta_2)^{1/2}\beta_1+(E_1+E_2)[(\beta_1)^{1/2}+(\beta_2)^{1/2}]\}\}\\
&+y^4\{\beta_1\beta_2+E_1E_2+(E_1+E_2)[\beta_1+\beta_2+4(\beta_1\beta_2)^{1/2}]-(\beta_2A_2+\beta_1A_1)-|V_{12}|^2\}\\
&+y^3\{2(E_1+E_2)[(\beta_2)^{1/2}\beta_1+(\beta_1)^{1/2}\beta_2]+2E_1E_2[(\beta_1)^{1/2}+(\beta_2)^{1/2}]\\
&\quad-2[(\beta_1)^{1/2}\beta_2A_2+(\beta_2)^{1/2}\beta_1A_1]-2|V_{12}|^2[(\beta_1)^{1/2}+(\beta_2)^{1/2}]\}\\
&+y^2\{(E_1+E_2)\beta_1\beta_2+E_1E_2[\beta_1+\beta_2+4(\beta_1\beta_2)^{1/2}]-\beta_1A_1(\beta_2+E_2)-\beta_2A_2(\beta_1+E_1)\\
&\quad-|V_{12}|^2[\beta_1+\beta_2+4(\beta_1\beta_2)^{1/2}]+2V_{12}r(A_1A_2\beta_1\beta_2)^{1/2}\}\\
&+y^1\{2E_1E_2[(\beta_1)^{1/2}\beta_2+(\beta_2)^{1/2}\beta_1]-2[E_1\beta_2A_2(\beta_1)^{1/2}+E_2\beta_1A_1(\beta_2)^{1/2}]\\
&\quad-2|V_{12}|^2[(\beta_1)^{1/2}\beta_2+(\beta_2)^{1/2}\beta_1]+2V_{12}r(A_1A_2\beta_1\beta_2)^{1/2}[(\beta_1)^{1/2}+(\beta_2)^{1/2}]\}\\
&+y^0\{E_1E_2\beta_1\beta_2-E_1\beta_1\beta_2A_2-E_2\beta_1\beta_2A_1+\beta_1\beta_2A_1A_2-r^2\beta_1\beta_2A_1A_2\\
&\quad-|V_{12}|^2\beta_1\beta_2+2V_{12}r(A_1A_2)^{1/2}\beta_1\beta_2\}\ .\end{aligned} \tag{4.4}$$

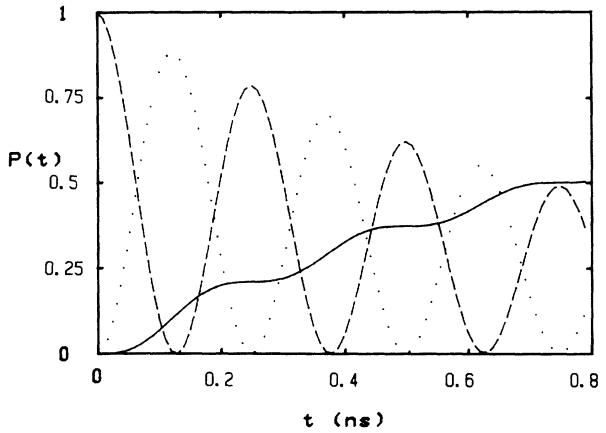

FIG. 4. Solid curve shows the probability of the electron's being in the continuum $\{|E\rangle\}$ a time t after the laser is turned on. The dashed and dotted lines show the populations of states $|1\rangle$ and $|2\rangle$, respectively. Parameters that are not as in Figs. 2 and 3 are $A_2=0.01$ cm^{-1} (so that the autodetaching rate is small compared with that of Figs. 2 and 3), $I=1.00\times10^6$ W/cm^2. The laser detuning is zero, i.e., $E_1=E_2$.

Figure 4 shows the time development of the populations for a case in which the coupling between the two discrete states is strong compared to the other couplings (i.e., for large q). The population of the continuum, which we have calculated as $1-|\langle 1|\psi(t)\rangle|^2-|\langle 2|\psi(t)\rangle|^2$, increases nonlinearly in a familiar staircase form[44] as the electron population undergoes Rabi cycling between the two discrete states. [Throughout this work we shall refer to the time t population of the continuum $\{|E\rangle\}$ as the time t photodetachment probability. We note, however, that if the laser is turned off at time t and if the state $|2\rangle$ is autodetaching, then the population of $|2\rangle$ will subsequently decay into the continuum, increasing the detachment probability to $1-|\langle 1|\psi(t)\rangle|^2$.]

For the parameters of Fig. 4, the probability of detachment increases to a final value of 1 at times beyond the range of the graph. However, for other parameters, it is possible to trap population within the discrete states, so that even the long-time photodetachment probability is less than unity.

Before discussing in detail how the trapping phenomena arise in our formalism, we briefly review the usual resolvent description of the decay of a single prepared state $|1\rangle$.[45] The matrix element of the Green's operator, $\langle 1|G(z)|1\rangle$, when considered as a function of the complex coordinate z, has a cut running from the threshold of the continuum (which for us will be $E=0$) to infinity along the positive real axis. Because of the cut there is more than one Riemann sheet, and, if the state can decay into the continuum, then $\langle 1|G(z)|1\rangle$ has a pole z_1, near E_1, in the fourth quadrant of the second Riemann sheet. This pole can be thought of as representing the decaying state $|1\rangle$—its real part gives the energy of state $|1\rangle$ (as shifted by the interactions considered) and its imaginary part gives half the width or decay rate of the state (in units where $\hbar=1$). The pole z_1 is the z which solves the equation

$$z-E_1-\Sigma^{11}(z)=0\ ,$$

where $\Sigma^{11}(z)$ has different forms on the two sheets. The state is at the threshold of the continuum and thus at a point of stabilization if $z_1=0$. Such a solution occurs if $-E_1-\Sigma^{11}(0)=0$. In the present work we have chosen our couplings so that $\Sigma^{jj}(0)=-A_j$. For a one discrete state system satisfying this condition, the shifted state will lie at the threshold of the continuum if $E_1=A_1$. It will decay if $E_1>A_1$, but will be stable if $E_1<A_1$. Further, if E_1 is close to threshold and $\mathrm{Re}\Sigma^{11}(z)$ is slowly varying in the vicinity of $z=0$, then E_1-A_1 will provide a first approximation to the energy of the state.

In describing the decay of two coupled states one typically finds two poles in the fourth quadrant of the second sheet, which can be interpreted in terms of decaying dressed states, with again real parts corresponding to energies of the dressed states and imaginary parts corresponding to half the decay rates. These poles are the poles of the projected resolvent operator $QG(z)Q$ of Eq. (2.8) and are the solutions of $\det\{Q[z-H^0-\Lambda(z)]Q\}=0$. In this context a dressed state becomes stable when the imaginary part of the pole goes to zero, i.e., when there is a solution for real $z_j\le0$ or for $z_j=E-i0$ for some $E>0$. If we make the change of variable $y=-iz^{1/2}$, then the first Riemann sheet of the z plane is mapped to the right half ($\mathrm{Re}y>0$) of the y plane, and the second sheet to the left half of the y plane. A pole z_j in the fourth quadrant of the second sheet of the z plane, representing a decaying state, is mapped to a pole y_j in the third quadrant of the y plane. The trapping condition $z_j=E-i0$ is replaced by $y_j=-i\sqrt{E}$. A pole on the negative real axis of the first sheet of the z plane, which can represent a stable state below threshold, will be mapped to the positive real axis of the y plane.

The complex dressed state energies for our system can be obtained by numerically finding the solutions of $D(y)=0$. There will, in general, be eight roots of the polynomial, but in most situations it is simple to identify the two that can be thought as relating to the energies of the complex dressed states. A convenient method of plotting the dependence of the energies and decay rates of the decaying states on a parameter such as the laser intensity I is to superpose plots[32,34] of $\mathrm{Re}(z_j)$ versus I and $\mathrm{Re}(z_j)\pm|\mathrm{Im}(z_j)|$ versus I. In Fig. 5 we plot the energies and widths of the complex decaying dressed states versus laser intensity for certain atomic parameters and fixed laser frequency, while in Fig. 6 we plot the energies and widths as a function of E_1 (and thus the laser frequency) for fixed laser intensity and the same atomic parameters. The energies and widths plotted were obtained by mapping the two roots of $D(y)$ that we identified as representing the dressed states from the y plane to the z plane (to $z_j=-y_j^2$). In Fig. 6, a third root is also drawn (using a curve with short dashes) for laser tunings less than 64 cm^{-1}. This third root lies on the negative real axis of the second Riemann sheet. The stabilization of the upper state at the Fano minimum and the stabilization or desta-

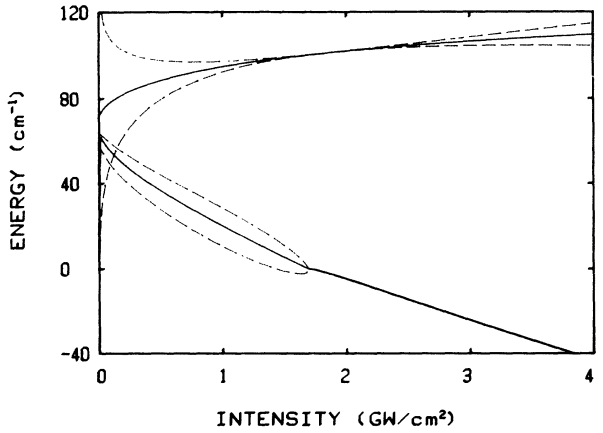

FIG. 5. Dressed state energies $\mathrm{Re}(z_j)$ (solid lines) vs laser intensity. The dashed lines give information about the dressed state half-widths $|\mathrm{Im}(z_j)|$—the upper curves give $\mathrm{Re}(z_2)\pm 25|\mathrm{Im}(z_2)|$, and the lower curves $\mathrm{Re}(z_1)\pm 2.5|\mathrm{Im}(z_1)|$. (The multiplicative factors of 2.5 and 25 are merely included for graph clarity.) Parameters that differ from those of Fig. 2 are $A_1/I=2\times 10^{-8}$ cm^{-1}/(W/cm^2), $V_{12}/\sqrt{I}=-6.73\times 10^{-4}$ cm^{-1}/(W/cm^2)$^{1/2}$, $A_2=10$ cm^{-1}, $\beta_2=0.4$ eV, $E_2=0.01$ eV$=80.65$ cm^{-1}. The detuning E_1-E_2 is -16 cm^{-1}. The upper state has width zero $[\mathrm{Im}(z_2)=0]$ at (to three significant figures) $I=1.85\times 10^9$ W/cm^2. [The upper curve does not have $\mathrm{Re}(z_2)=E_2$ in the limit $I\to 0$ because the autodetaching interaction shifts the state slightly.] For these atomic parameters, $q(E_2)=-6.19$.

bilization of the lower state at continuum threshold (i.e., at dressed state energy zero) are both clearly visible in the graphs. (In order to demonstrate the state-shifting effect clearly while keeping the laser intensity below 10 GW/cm^2, we have increased the values of A_1/I and $V_{12}/\sqrt{I}$ from those used in the earlier figures.) Under certain conditions it is possible for both the complex dressed states to be stable, i.e., for both trapping conditions to be met simultaneously. This occurs in Fig. 5 at laser intensity 1.85 GW/cm^2 (to three significant figures), but does not occur in Fig. 6. We note that this the "double trapping" phenomenon can only occur if at low intensities both states lie between the continuum threshold and the Fano minimum. This condition requires $q<0$.

The roots near the continuum threshold exhibit interesting behavior near the stabilization intensity or frequency. For example, the root representing the lower state of Fig. 5 does not move directly from the fourth quadrant of the second Riemann sheet through threshold onto the negative real axis of the first sheet as the laser intensity increases. Instead, and prior to stabilization, it moves from the fourth quadrant of the second sheet into the third quadrant of the second sheet, and then onto the negative real axis of the second sheet. There is also a conjugate root which moves from the first quadrant of the second sheet into the second quadrant of the second sheet, and then onto the negative real axis. These two roots then move in opposite directions along the negative real axis. One of them moves to the origin, and then moves back along the negative real axis of the first sheet. (This effect is barely discernible on the graph where there is a small "bump" near where the lower state crosses $E=0$.) The other root, which is not shown on the graph, moves away from the origin on the real axis of the second sheet. The motion is simpler in the y plane—conjugate zeros come together on the negative real axis, and then move apart along the real axis, with one of them moving through the origin onto the positive real axis. Thus, if one thinks of the roots as representing the decaying states, we have for certain intensities the interesting phenomenon of a state lying below the continuum threshold, but maintaining a nonzero width.

The root(s) representing the lower state in Fig. 6 exhibits similar interesting behavior. A closeup of the behavior near the destabilization threshold is shown in Fig. 7. For laser tunings less than 64.0 cm^{-1}, there is a root on the negative real axis of the physical sheet; this root is

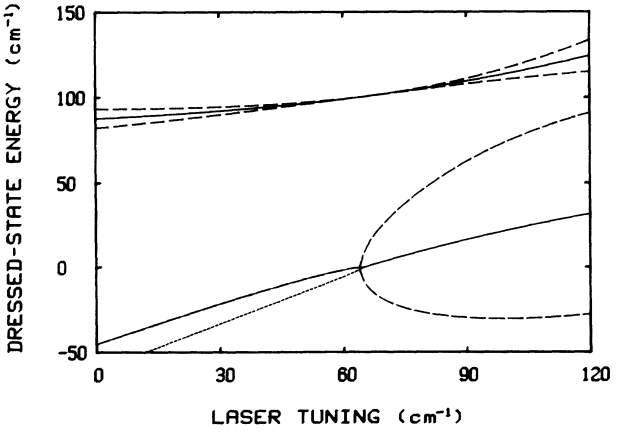

FIG. 6. Dressed state energies $\mathrm{Re}(z_j)$ (solid and fine dashed curves) and $\mathrm{Re}(z_j)\pm 10|\mathrm{Im}(z_j)|$ (long dashes) vs E_1 (the laser tuning relative to the continuum edge) for laser intensity $I=1.71$ GW/cm^2. Other parameters are as in Fig. 5. Second sheet roots for which $\mathrm{Re}(z_j)<0$ are denoted by the fine dashed curves.

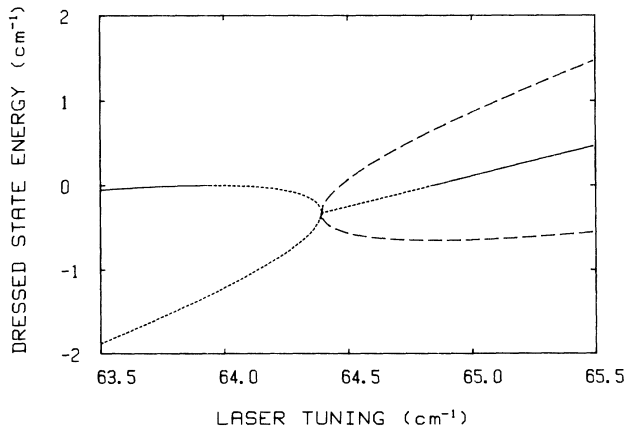

FIG. 7. Closeup of the "threshold" region of Fig. 6, showing $\mathrm{Re}(z_j)\pm|\mathrm{Im}(z_j)|$ vs E_1.

denoted by the solid curve in Figs. 6 and 7. There is also a root on the negative real axis of the nonphysical sheet; this root is denoted by the curve with short dashes in the lower left of the figure. At 64.0 cm^{-1}, the first root reaches the origin, and then with increasing laser frequency, it moves back along the negative real axis of the second sheet until meeting the second root at tuning 64.4 cm^{-1}. The roots then separate and become conjugate roots in the second and third quadrants of the second sheet; they reach the first and second quadrants (i.e., have energy greater than zero) at tuning 64.8 cm^{-1}. In both Figs. 6 and 7, curves with short dashes denote second sheet roots which have negative real parts.

For completeness, we also include information on the locations of the other roots for the conditions of Figs. 5 and 6. The roots not mentioned above all lie on the negative real axis of the second Riemann sheet. None of them lie closer to the origin that 2800 cm^{-1} (0.35 eV).

Because of the complexity of $D(y)$, it is not a simple matter to predict analytically the conditions necessary for stabilization of the complex dressed states. However, one can show very simply that $D(y)$ has a root at $y=0$ (and thus $z=0$) at laser intensity I such that

$$I=\frac{E_1(E_2-A_2)}{[\nu r(A_2)^{1/2}-\mu]^2+\nu^2(E_2-A_2)}\ , \tag{4.5}$$

where

$$\nu^2=A_1/I,\quad \mu=V_{12}/\sqrt{I}\ .$$

Equation (4.5) clearly gives a positive I when (for example) E_1 and E_2-A_2 are both positive. (Since A_2 can be thought of as a shift of the upper state due to the configuration interaction with the continuum, the condition $E_2-A_2>0$ is equivalent to the condition that the upper discrete state lie above the threshold of the continuum for $I=0$.)

The trapping condition for the higher-energy dressed state is more difficult to write down. Numerically, the condition is not difficult to find because trapping can only occur at an energy equal to the energy of the Fano minimum,[37,38] which can be found by setting $\varepsilon(E)=-q(E)$, using Eqs. (3.5b) and (3.1), and solving the resulting equation for E. (All the laser intensity and frequency-dependent quantities cancel out, so that the location of the minimum is independent of laser parameters.) One then can set $y=-i\sqrt{E}$ in $D(y)$, and use the trapping condition $D(-i\sqrt{E})=0$ to obtain coupled linear equations for the laser intensity and frequency in terms of the various atomic parameters.

Figure 8 shows the photodetachment probability and the populations of the discrete states for the double trapping case (in which both the complex dressed states are stable) which occurs in Fig. 5 near laser intensity 1.85 GW/cm^2. In this case, the photodetachment probability rises to an asymptotic value of 0.36, and the trapped population oscillates indefinitely between the two states $|1\rangle$ and $|2\rangle$. We emphasize that these "stable dressed states" of the model arise not only through the interaction between the discrete states, but also through the interaction of the discrete states with the continuum. We note, for example, that if one were to neglect the interaction with the continuum, then one would expect the dressed states to be separated in energy by $\Delta E=[(E_1-E_2)^2+4V_{12}^2]^{1/2}$, which for the parameters of Fig. 8 is 60 cm^{-1} (7.4 meV). However, the pole locations are numerically found to be -2 cm^{-1} and $+101$ cm^{-1}, for a net energy separation of $\Delta E'=103$ cm^{-1} (12.8 meV). Correspondingly, the cycling time is not $2\pi\hbar/\Delta E=5.6\times10^{-13}$ s, but is $2\pi\hbar/\Delta E'=3.2\times10^{-13}$ s.

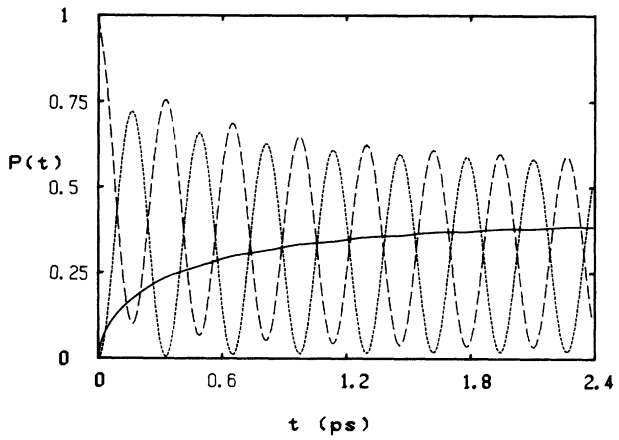

FIG. 8. In the case of double trapping, the probability of detachment rises quickly to a constant value. Rabi oscillations between the product states continue indefinitely. Atomic parameters are as in Fig. 5, with $I=1.85\times10^9$ W/cm^2.

It is not always possible to identify two of the roots of $D(y)$ as simply representing two decaying dressed states. To illustrate this difficulty, we show in Fig. 9 the motion of three of the roots of $D(y)$ with increasing laser intensity. At low laser intensities, two of the roots can be identified with the atom-field product states; each of these roots also has a conjugate root (of course, both the roots and their conjugates are on the second Riemann sheet), and the other three roots lie on the negative real axis of the second Riemann sheet. With increasing laser intensity, one of the "dressed state" roots moves toward lower energy, eventually having a real part less than zero while still maintaining a nonzero imaginary part. Simultaneously, one of the three second sheet negative real axis roots moves along the axis toward the origin. At an intensity of approximately 10.9 GW/cm^2, the two moving roots have equal real parts. As the intensity is increased further, the real axis pole moves to the origin and appears on the first sheet at the intensity given by Eq. (4.5). Meanwhile, the root with nonzero imaginary part continues to move toward lower energies; its imaginary part increases rapidly in absolute value once its real part is less than the real-axis zero. At high laser intensities, the pole which lies on the negative real axis of the first sheet can be thought of as representing a stable dressed state. However, during the "crossover" period, neither root can be identified as solely representing the lower dressed state, and both are important in calculating the discrete-state population amplitudes.

In Figs. 10 and 11 we show the time development of

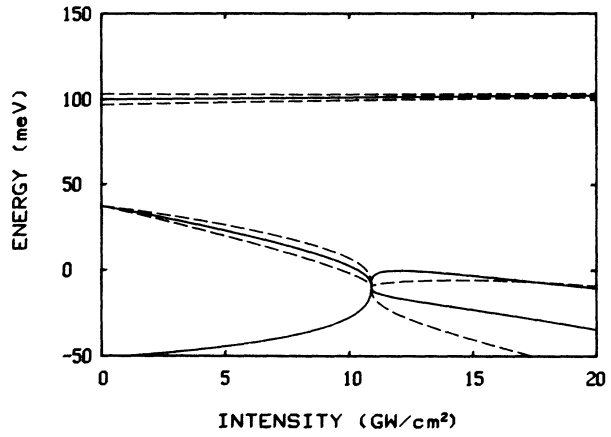

FIG. 9. $\mathrm{Re}(z_j)$ (solid curves) and $\mathrm{Re}(z_j)\pm 0.5|\mathrm{Im}(z_j)|$ (dashed curves) for three of the roots z_j of $D(y)$. Atomic parameters that differ from those of Fig. 3 are $A_1/I=2\times10^{-8}$ $\mathrm{cm}^{-1}/(\mathrm{W/cm}^2)$, $V_{12}/\sqrt{I}=-6.73\times10^{-4}$ $\mathrm{cm}^{-1}/(\mathrm{W/cm}^2)^{1/2}$. The laser detuning E_1-E_2 is -505 cm^{-1} (-63 meV). The two lower roots have equal real parts at intensity 10.9 $\mathrm{GW/cm}^2$. One of the roots moves in along the negative real axis of the second sheet until reaching the origin, and then moves out along the negative real axis of the first sheet. Another of the roots lies where the laser is tuned at weak intensities, but then is shifted continually downward with increasing laser intensity. Its minimum width occurs when its real part is equal to the real part of the root on the negative real axis, at -71 cm^{-1} (-8.8 meV), and is $|\mathrm{Im}(z_2)|=14.5$ cm^{-1} (1.80 meV). For these atomic parameters, $q=-0.93$.

the photodetachment probability for the system of Fig. 9, at laser intensities 11.1 and 11.5 $\mathrm{GW/cm}^2$, respectively. At the lower of these laser intensities, one root of $D(y)$ lies on the negative real axis of the second sheet, and one root lies in the third quadrant of the second sheet (i.e., it lies "below threshold," but maintains nonzero width); for this case all population is eventually transferred to the

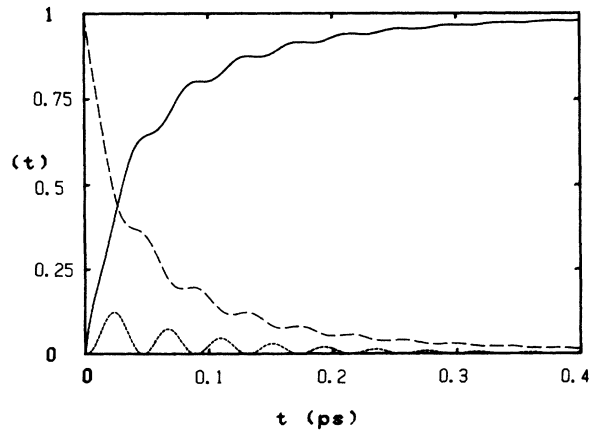

FIG. 10. Time development of the populations of state $|1\rangle$ (large dashes), state $|2\rangle$ (small dashes), and continuum $\{|E\rangle\}$ for the parameters of Fig. 9, at laser intensity 11.1 $\mathrm{GW/cm}^2$.

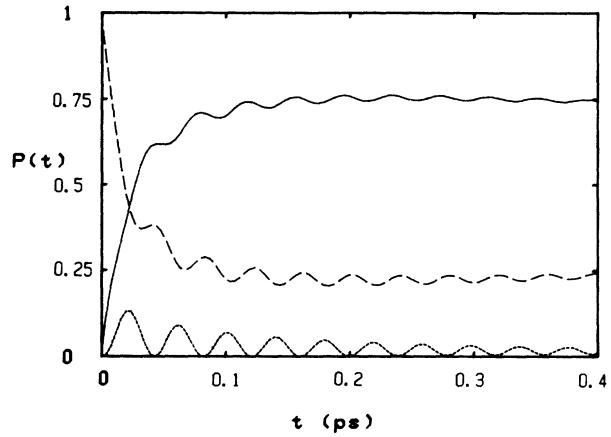

FIG. 11. Time development as in Fig. 10, except at laser intensity 11.5 $\mathrm{GW/cm}^2$, showing partial trapping of the population in the discrete states and decaying oscillations between the discrete states.

continuum. At the higher of these intensities, one of the roots lies on the negative real axis of the first sheet, and some population does not decay into the continuum. We note in Fig. 11 the decaying oscillations between the two discrete states; their populations eventually reach constant values of 0.26 and 0.02, reflecting their respective contributions to the single stable dressed state. We also note the oscillations in the total photodetachment probability. These latter oscillations are in contrast to detachment probabilities calculated in the pole approximation, in which the detachment probabilities display a staircase form,[44] such as in Fig. 4, and never decrease with increasing time.

We note in comparing Figs. 10 and 11 that there is no dramatic population trapping effect when one of the roots jumps onto the real axis. It has previously been shown[8,10] that for a single discrete state $|1\rangle$ coupled to a continuum $\{|\chi_E\rangle\}$ so that a bound state $|b\rangle$ of energy E_b is formed, the population of the bound state (for a system initially in $|1\rangle$) is given by

$$|\langle b|1\rangle|^2=\left[1+\int dE\frac{|\langle 1|V|\chi_E\rangle|^2}{(E_b-E)^2}\right]^{-1}. \tag{4.6}$$

It was also noted that in the limit $E_b\uparrow 0$ for an s-wave continuum, in which $|\langle 1|V|\chi_E\rangle|^2$ is proportional to $E^{1/2}$ for small energies, the integral in (4.6) diverges, so that $|\langle b|1\rangle|^2$ approaches zero. This result also applies for the model of interest in the present work, in which there is an autodetaching state $|2\rangle$ above the threshold of the continuum $|E\rangle$, since one can allow $|\chi_E\rangle$ to represent the structured continuum obtained by a diagonalization of the $|2\rangle-\{|E\rangle\}$ system—it is simple to show that[46]

$$\langle 1|V|\chi_E\rangle=\langle 1|V|E\rangle+\frac{[\langle 1|V|E\rangle+\Sigma^{12}(E+i0)]\langle 2|V|E\rangle}{E-E_2-\Sigma^{22}(E+i0)}, \tag{4.7}$$

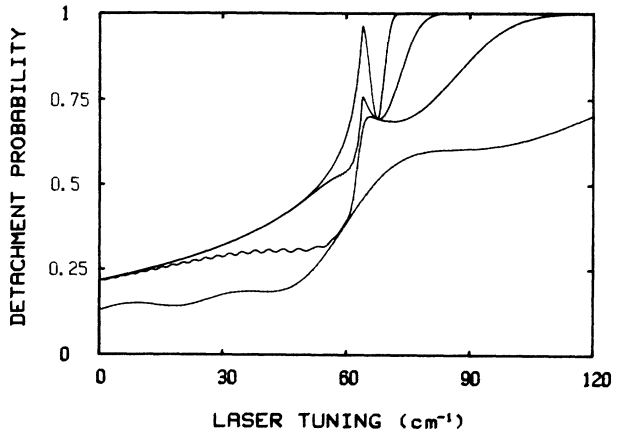

FIG. 12. Photodetachment probability vs laser tuning (E_1) for the conditions of Fig. 6, at times (from bottom to top) 2×10^{-12} s, 2×10^{-11} s, 2×10^{-10} s, and 2×10^{-9} s.

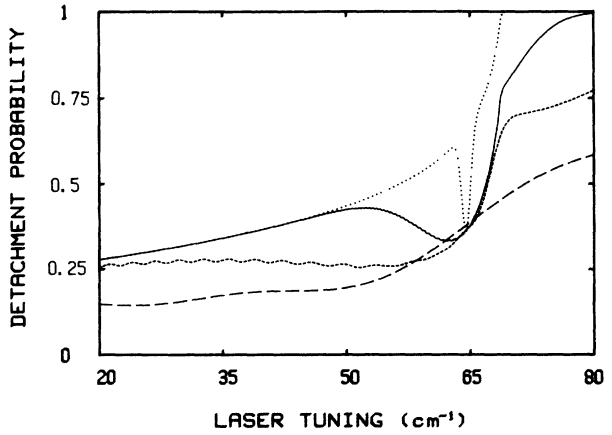

FIG. 13. Photodetachment probability vs laser tuning (E_1) for the conditions of Fig. 8, at times 2×10^{-12} s (long dashes), 2×10^{-11} s (short dashes), 2×10^{-10} s (solid), and 2×10^{-8} s (dotted). The frequency matches that used in Fig. 8 at 64.6 cm^{-1}. At longer times, the curve matches that of $t=2\times10^{-8}$ s, except that the dip at 64.6 cm^{-1} (the frequency of "double trapping" and of Fig. 8) becomes progressively narrower.

which satisfies the necessary condition $|\langle 1|V|\chi_E\rangle|^2 \propto E^{1/2}$ for small energies. One might expect a more dramatic effect for coupling to a p-wave continuum.

In Fig. 12 we plot the detachment probability versus E_1 for the conditions of Fig. 6 for several different times. The curves display a number of interesting features. The destabilization of the lower state between 60 and 65 cm^{-1} is clearly visible, but there is no single frequency which marks a boundary between a stable region in which appreciable population is trapped in the ion even at long times and an unstable region in which the ion is completely detached at long times. This lack of a boundary is consistent with the observation above that a state at the origin should have zero population in our model. The partial trapping that occurs when one of the dressed states lies at the Fano minimum is also clearly visible. At "intermediate" times there is a broad dip in the detachment probability, reflecting the narrowing of the upper dressed state. With increasing time, the dip becomes progressively more narrow, but continues to drop to the same value ($P=0.69$).

In Fig. 13 we plot the photodetachment probability versus E_1 for the conditions of Fig. 8 and various times. For those conditions, both dressed states are stable at $E_1=64.6$ cm^{-1}, and at this frequency the detachment probability drops to 0.36 (the asymptotic value of the photodetachment probability of Fig. 8). As for Fig. 12, we note that there is no abrupt "threshold boundary" at which the detachment probability jumps abruptly to one in the long-time limit.

In all the above examples, we have assumed that at zero laser intensity the excited discrete state lay above the threshold of the continuum and was autodetaching. We consider now a case in which the upper state lies slightly below the threshold of the continuum. In this case it is possible for the laser coupling between the discrete states to shift the state above the threshold of the continuum. This is illustrated in Fig. 14. We have chosen the laser frequency so that in the limit of zero laser intensity (but still including the configuration interaction between the upper state and the continuum) the two states are degenerate in energy. As the intensity increases from zero, the two states are shifted apart, and eventually one is pushed above the threshold of the continuum. In Fig. 15 we show the time development of the populations for intensity 3 GW/cm^2, when both states lie below the threshold; the oscillations continue indefinitely. In Fig. 16 we show the time development for intensity 10 GW/cm^2, when one of the dressed states has been pushed above threshold. Now the detachment probability

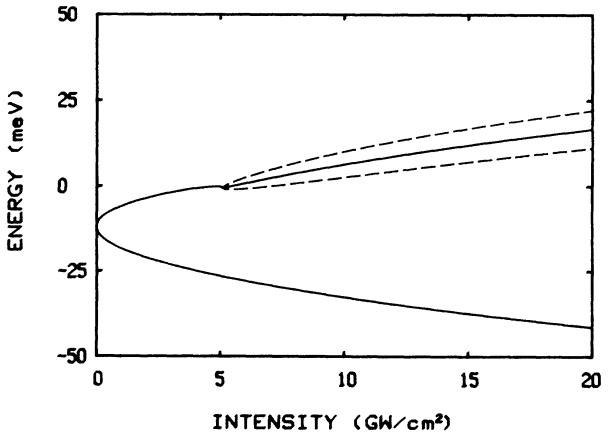

FIG. 14. $\mathrm{Re}(z_j)$ (solid curves) and $\mathrm{Re}(z_j)\pm|\mathrm{Im}(z_j)|$ (dashed curves) for the roots of $D(y)$ which represent complex dressed states. Atomic parameters that differ from those of Fig. 2 are $E_2=-5.00$ meV (-40.3 cm^{-1}), $V_{12}/\sqrt{I}=1.79\times10^{-3}$ $cm^{-1}/(W/cm^2)^{1/2}$. The laser detuning E_1-E_2 is -55.3 cm^{-1} (-6.86 meV). The configuration interaction between the upper state and the continuum shifts the upper state downward by 55.3 cm^{-1}, so that in the limit of low laser intensity, the two dressed or product states are degenerate in energy.

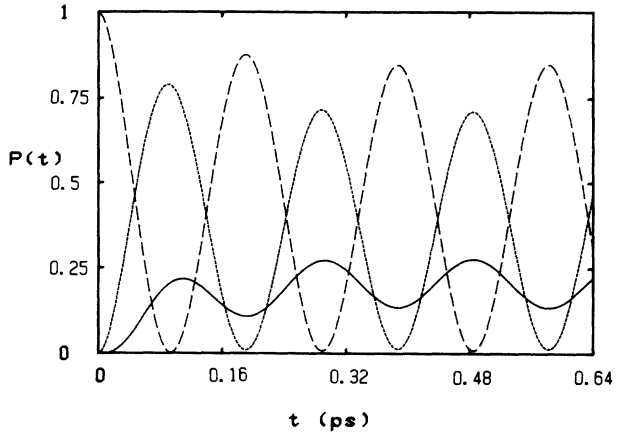

FIG. 15. Time development of the populations of state $|1\rangle$ (large dashes), state $|2\rangle$ (smaller dashes), and the continuum (solid curve), for the conditions of Fig. 14 at laser intensity $I=3.0$ GW/cm^2. Since both dressed states have $\mathrm{Im}(z_j)=0$, the oscillations continue indefinitely.

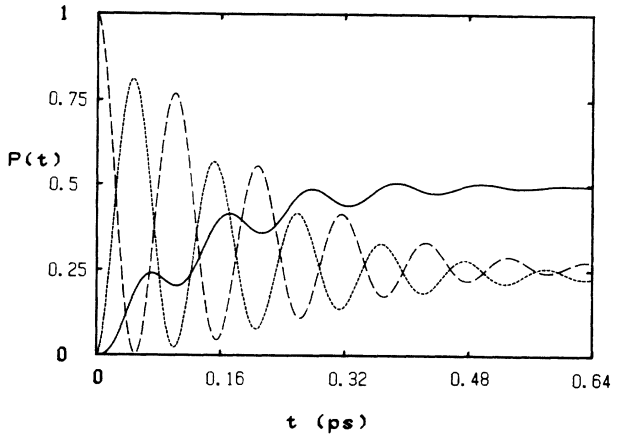

FIG. 16. Time development of the populations of state $|1\rangle$ (large dashes), state $|2\rangle$ (smaller dashes), and the continuum (solid curve), for the conditions of Fig. 14 at laser intensity $I=10.0$ GW/cm^2.

reaches as asymptotic value of 0.50, and the discrete state populations each approach 0.25, representing their contributions to the stable dressed state.

V. SUMMARY AND DISCUSSION

We have presented an exact solution of the time-dependent Schrödinger equation for a model system containing two discrete states and one s-wave photodetachment continuum. We have shown explicitly that the pole approximation is not a valid approximation near the threshold of the continuum. We have examined the time development of the populations and have observed that transitions to the continuum are not irreversible. We have examined population trapping effects for our model system, and have observed that such effects can arise through either a shift of a dressed state below the threshold of the continuum or a shift of a dressed state through the Fano minimum. We have also observed that under certain conditions, both trapping conditions can be met simultaneously. Under other conditions, the model features a "decaying dressed state" with energy below the lowest energy of the continuum. We have noted that at high laser intensities there is no unambiguous minimum laser frequency needed to detach the electron—there is instead a smooth transition from partial photodetachment to total photodetachment as the laser frequency is increased. Finally, we have shown that for the case in which the excited state of the negative ion lies below the threshold of the continuum, the laser interaction between the two discrete states can be used to shift the upper state above the threshold of the continuum, where it can decay through autodetachment. Our studies have involved an s-wave continuum only. One can expect qualitatively similar results for continua with other angular momenta, although some behavior very close to threshold could be strongly influenced by replacing the $E^{1/2}$ dependence of Eq. (2.2) with a smoother $E^{3/2}$ or $E^{5/2}$ dependence. Details of such effects will be considered elsewhere.

While we have presented an exact solution for our model, it must be remembered that a number of effects were neglected in choosing the model. Indeed, some of the effects we have studied within the model (such as the behavior of the dressed states shown in Fig. 7) are in fact smaller than other effects which have been ignored in the model. These other effects would need to be included in any complete description of the photodetachment process within a real negative ion.

ACKNOWLEDGMENTS

The work of S.H. and M.W. was supported by a William and Flora Hewlett Foundation Grant of Research Corporation, by the National Science Foundation through Grant No. PHY-8711639, and by Calvin College. The work of J.C. was supported by the National Science Foundation through Grant No. PHY86-04504 to the University of Colorado.

*Present address: Department of Physics and Astronomy, University of Maryland, College Park, MD 20742.

[1]J. Javanainen, Opt. Commun. **46**, 175 (1983).

[2]A. Raczynski and J. Zaremba, J. Phys. B **19**, 3895 (1986); **20**, 1919 (1987); Phys. Rev. A **36**, 5078 (1987); **38**, 5115 (1988).

[3]G. Alber and P. Zoller, Phys. Rev. A **37**, 377 (1988).

[4]C. Cohen-Tannoudji and P. Avan, Colloq. Int. C.N.R.S. **273**, 93 (1977).

[5]S. E. Kumekov and V. I. Perel, Zh. Eksp. Teor. Fiz. **81**, 1693 (1981) [Sov. Phys.—JETP **54**, 899 (1981)].

[6]K. Rzazewski, M. Lewenstein, and J. H. Eberly, J. Phys. B **15**, L661 (1982).

[7]Z. Bialynicka-Birula, Phys. Rev. A **28**, 836 (1983); J. Phys. B **16**, 4351 (1983).

[8]A. E. Kazakov and M. V. Federov, Zh. Eksp. Teor. Fiz. **83**, 2035 (1982) [Sov. Phys.—JETP **56**, 1179 (1982)]; M. V. Federov and A. Kazakov, J. Phys. B **16**, 3641 (1983); **16**, 3653 (1983); A. I. Andrjushinn, M. V. Federov, and A. E. Kazakov, *ibid.* **17**, 3469 (1984).

[9]J. Javanainen, J. Phys. B **16**, 1343 (1983).

[10]S. L. Haan and J. Cooper, J. Phys. B **17**, 3481 (1984).

[11]K. S. Lam and T. F. George, Phys. Rev. A **33**, 2491 (1986).

[12]A. B. Voitkiv and V. A. Pazdzersky, J. Phys. B **19**, 1633 (1986); **21**, 937 (1988).

[13]M. Kutzner, H. P. Kelly, D. J. Larson, and Z. Altun, Phys. Rev. A **38**, 5107 (1988).

[14]See, for example, P. Agostini and G. Petite, Contemp. Phys. **29**, 57 (1988), and references therein.

[15]R. Trainham, G. D. Fletcher, N. B. Mansour, and D. J. Larson, Phys. Rev. Lett. **59**, 2291 (1987); see also P. S. Armstrong, T. Olsson, and D. J. Larson, Bull. Am. Phys. Soc. **34**, 1398 (1989).

[16]P. Lambropoulos and P. Zoller, Phys. Rev. A **24**, 379 (1981). See also P. Lambropoulos, Appl. Opt. **19**, 3926 (1980).

[17]Y. I. Geller and A. K. Popov, Pis'ma Zh. Tekh. Fiz. **7**, 719 (1981) [Sov. Tech. Phys. Lett. **7**, 307 (1981)].

[18]V. I. Maatveev and E. S. Parilis, Zh. Tekh. Fiz. **51**, 1792 (1981) [Sov. Phys. Tech. Phys. **26**, 1039 (1981)].

[19]K. Rzazewski and J. H. Eberly, Phys. Rev. Lett. **47**, 408 (1981); Phys. Rev. A **27**, 2026 (1983); J. H. Eberly, K. Rzazewski, and D. Agassi, Phys. Rev. Lett. **49**, C693 (1982); D. Agassi, K. Rzazewski, and J. H. Eberly, Phys. Rev. A **28**, 3648 (1983).

[20]A. I. Andryushin, M. V. Federov, and A. E. Kazakov, J. Phys. B **15**, 2851 (1982); Opt. Commun. **49**, 120 (1984); A. I. Andryushin, A. E. Kazakov, and M. V. Federov, Zh. Eksp. Teor. Fiz. **82**, 91 (1982) [Sov. Phys.—JETP **55**, 53 (1982)]; A. I. Andryushin and A. E. Kazakov, J. Phys. B **18**, 1501 (1983).

[21]P. T. Greenland, J. Phys. B **15**, 3191 (1982).

[22]A. Lami and M. K. Rahman, Opt. Commun. **43**, 383 (1982); Phys. Rev. A **26**, 3360 (1982).

[23]J. Zakrzewski, J. Phys. B **17**, 719 (1984).

[24]S. F. Li and F. C. Lin, J. Phys. B **22**, 1183 (1989).

[25]G. S. Agarwal, S. L. Haan, K. Burnett, and J. Cooper, Phys. Rev. Lett. **48**, 1164 (1982); Phys. Rev. A **26**, 2277 (1982); S. L. Haan and G. S. Agarwal, in *Spectral Line Shapes Volume 2*, Proceedings of the Sixth International Conference, Boulder, 1982, edited by K. Burnett (De Gruyter, Berlin, 1983), p. 1013; G. S. Agarwal, S. L. Haan, and J. Cooper, Phys. Rev. A **29**, 2552 (1984); **29**, 2565 (1984); Phys. Rev. Lett. **52**, 1480 (1984).

[26]M. Crance and L. Armstrong, Jr., J. Phys. B **15**, 3199 (1982).

[27]G. S. Agarwal and D. Agassi, Phys. Rev. A **27**, 2254 (1983).

[28]M. Lewenstein, J. W. Haus, and K. Rzazewski, Phys. Rev. Lett. **50**, 417 (1983); J. W. Haus, M. Lewenstein, and K. Rzazewski, Phys. Rev. A **28**, 2269 (1983).

[29]V. A. Pazdzersky and A. B. Voitkiv, J. Phys. B **18**, 1495 (1985).

[30]D. Agassi and J. H. Eberly, Phys. Rev. A **34**, 2843 (1986).

[31]U. Fano, Phys. Rev. **124**, 1866 (1961).

[32]P. E. Coleman, P. L. Knight, and K. Burnett, Opt. Commun. **42**, 171 (1982); P. E. Coleman and P. L. Knight, J. Phys. B **15**, L235 (1982); **15**, 1957 (1982).

[33]B. Dai and P. Lambropoulos, Phys. Rev. A **36**, 5205 (1987).

[34]P. L. Knight, Comments At. Mol. Phys. **15**, 193 (1984).

[35]Z. Deng and J. H. Eberly, J. Opt. Soc. Am. B **1**, 102 (1984).

[36]A. Lami and N. K. Rahman, Phys. Rev. A **33**, 782 (1986); **34**, 3908 (1986).

[37]E. Kyrola, J. Phys. B **19**, 1437 (1986).

[38]S. L. Haan and G. S. Agarwal, Phys. Rev. A **35**, 4592 (1987).

[39]E. P. Wigner, Phys. Rev. **73**, 1002 (1948).

[40]See, for example, S. L. Haan and V. L. Jacobs, Phys. Rev. A **40**, 80 (1989).

[41]I. S. Gradshteyn and I. M. Ryzhik, *Table of Integrals, Series and Products* (Academic, Orlando, 1980).

[42]S. L. Haan, Phys. Rev. A **40**, 4344 (1989).

[43]*Handbook of Mathematical Functions,* Natl. Bur. Stand. Appl. Math. Ser. No. 55, edited by M. Abramowitz and I. Stegun (U.S. GPO, Washington, D.C., 1964).

[44]B. L. Beers and L. Armstrong, Jr., Phys. Rev. A **12**, 2447 (1975).

[45]See, for example, M. L Goldberger and K. M. Watson, *Collision Theory* (Wiley, New York, 1964).

[46]S. L. Haan and J. Cooper, Phys. Rev. A **28**, 3349 (1983).